Structure and photoluminescence properties of fishbone-like $PbMoO_4$ nanostructures obtained via the surfactant-assisted hydrothermal method

Runping Jia (贾润萍)* and Kangsheng Zheng (郑康生)

School of Materials Science and Engineering, Shanghai Institute of Technology, Shanghai 201418, China

**Corresponding author: jrpchem@yahoo.com.cn*

Received June 13, 2012; accepted August 7, 2012; posted online September 28, 2012

Fishbone-like $PbMoO_4$ nanostructures are successfully obtained via the surfactant-assisted hydrothermal method at 160 °C. Polyethylene glycol (PEG2000) is used as the template agent. The nanostructures are characterized via X-ray diffraction, field-emission scanning electron microscopy, Fourier transform infrared spectroscopy, ultraviolet-visible light (UV-Vis) spectroscopy, and photoluminescence (PL) measurements. The $PbMoO_4$ morphology is highly associated with the molecular nature of PEG2000. $PbMoO_4$ nanoparticles obtained from PEG2000 have a fishbone-shaped, scheelite-type tetragonal structure, in which numerous secondary branches vertically grow on both sides of the main stem. The structures exhibit broad PL emission bands with the maximum at 306 and 390 nm when excited at 250 nm. In addition, the UV-Vis absorption edge of the structures is in the 280 to 310 nm region, and the band gap is 4.07 eV. A plausible formation mechanism for the fishbone-like $PbMoO_4$ nanostructures is also discussed.

OCIS codes: 160.2540, 160.4236, 160.4670.

doi: 10.3788/COL201210.111603.

The scheelite -type family of molybdates and tungstates has been extensively investigated to obtain new functionalities and behaviors associated with a broad range of properties[1−3]. Lead molybdate ($PbMoO_4$) belongs to this family and is a promising material for industrial applications such as acoustic-optical deflectors, modulators, ion conductors, and low-temperature scintillators in nuclear instruments[4−7].

In the past decades, $PbMoO_4$ crystals were prepared mainly via the solid-state reaction and Czochralski crystal growth, which usually require complex experimental procedures, sophisticated equipment, and harsh synthesis conditions[8,9]. Recently, the controlled synthesis of molybdate crystallites with desirable shapes, sizes, and crystal structures have become of considerable interest because of its wide range of technological applications[10]. Several wet-chemical solution methods such as microwave irradiation have been developed. However, some of these methods have verified serious problems, including polydispersed particle size distribution and uncontrolled morphology[11−13]. Thus, the controllable synthesis of $PbMoO_4$ crystals with homogenous and well-defined morphologies via facile routes remains a significant challenge.

Complex nanostructures have unique optical and electronic properties because of their morphologies and spatial organization[14,15]. In this study, a novel, fishbone-like $PbMoO_4$ nanostructure was synthesized via a simple polyethylene glycol (Mw 2000) (PEG2000)-induced hydrothermal approach. PEG2000 is often used as a template in nano- and microcrystal fabrication. These distinct fishbone-like $PbMoO_4$ nanoproducts have potential applications in the fabrication of electronic and optoelectronic nanodevices.

For the hydrothermal reaction, the reagents were of analytical grade and used as received. In a typical synthesis, 11.124-g $PbCl_2$ and 9.678-g $Na_2MoO_4{\cdot}2H_2O$ were separately dissolved in 40-mL hot water and transferred into two separate 100-mL flasks. Water was then added to the graduation mark to obtain 0.4 mol/L solutions. Afterward, 3 mL of the as-prepared $PbCl_2$ solution, 0.2-g PEG2000, and 30-mL water were successively added into a 50-mL flask under vigorous stirring. An equimolar Na_2MoO_4 solution was then added into the mixture, which was subsequently ultrasonically treated for 30 min (frequency, 40 kHz). The resulting white solution was transferred into a 50-mL Teflon-lined stainless steel autoclave. The sealed tank was heated to 160 °C and maintained at this temperature for 4 h without shaking or stirring. The solution was then collected and naturally cooled to room temperature. The resulting white precipitate was washed three times with distilled water and absolute alcohol to remove the reactant residues and then preserved in absolute alcohol for further characterization.

The crystalline phase was identified via X-ray diffraction (XRD) using a Rigaku D/max2550 diffractometer with Cu-Kα radiation ($\lambda = 0.15418$ nm). The sample morphology was observed under an FEI Quanta 200F field-emission scanning electron microscope (SEM). The Fourier transform infrared (FTIR) spectra of KBr powder-pressed pellets were recorded with a Nicolet NEXUS870 FTIR spectrometer (USA). Photoluminescence (PL) and UV-visible light (UV-Vis) spectra were obtained using a Perkin-Elmer luminescence spectrophotometer (LS-55, USA) and an Agilent 8453 UV- Vis spectrophotometer, respectively.

The as-synthesized product was first analyzed via SEM. The corresponding low- and high-magnification SEM images are shown in Fig. 1. The low-magnification image of the product (Fig. 1(a)) shows an interesting fishbone-like morphology, with no trace of any other morphology. The high-magnification SEM images (Figs. 1(b) and 1(c)) verify this morphology. Figure 1(c) shows

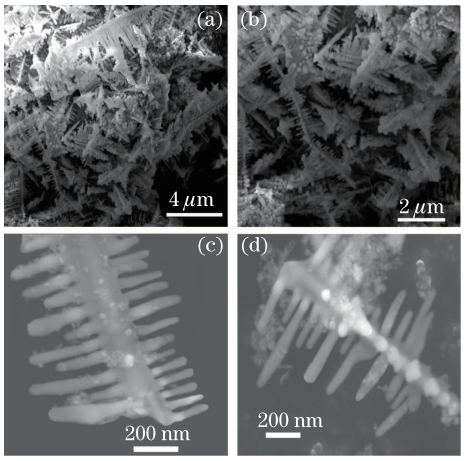

Fig. 1. SEM images of fishbone-like $PbMoO_4$ nanostructures at (a) low-, (b) medium-, and (c) high-magnifications. (d) Typical broken fishbone nanostructure.

that the main spine is several micrometers long. Both sides of this spine are covered with several uniformly distributed secondary branches (length: ~400 nm; widths: 40 to 80 nm). This unique, fishbone-like $PbMoO_4$ nanostructures are considerably different from the previously reported nanoplates[14], indicating that PEG2000 is vital to $PbMoO_4$ shape control. Most of the large products consist of small pieces such as those shown in Fig. 1(d). These products may have developed at a later stage of the hydrothermal process as a result of vigorous movement and impingement of the fishbone under a high-temperature and high-pressure environment, which in turn led to the formation of a large amount of broken fishbone.

$PbMoO_4$ crystals exhibit a ($I4_1/a$) space group, which belongs to a tetragonal structure that consists of tetrahedral [MoO_4] clusters and deltahedral [PbO_8] clusters[16]. XRD was used to analyze the phase structure of the as-grown product; the results are shown in Fig. 2. All the diffraction peaks in the XRD pattern can be identified to the scheelite-type tetragonal $PbMoO_4$ structure. This result is in agreement with that of the standard JCPDS card No. 44-1486 [space group $I4_1/a$][17], with lattice parameters of $a = b = 0.5433$ nm, $c = 1.202$ nm, and $\alpha = \beta = \gamma = 90°$. No impurities were detected. The sharp XRD peaks imply high sample crystallinity. These results indicate the successful fabrication of the phase-pure $PbMoO_4$ tetragonal structure via the proposed process.

Based on the broadening behavior of the XRD peaks, the widths of the secondary branches were estimated using the Scherrer equation, $D = 0.941\lambda/\beta\cos\theta$, where D is the average grain size, λ is the X-ray wavelength (0.154 05 nm), and θ and β are the diffraction angle and full-width at half-maximum (FWHM, in radian) of an observed peak, respectively[18]. The diffraction peak at $2\theta = 26.9761°$, which is associated with the (112) crystallographic plane, was used to calculate the widths of the secondary branches. The calculated average values were approximately 38.5 nm, which is in high agreement with the obtained SEM results.

$PbMoO_4$ crystals have 26 distinct vibration modes similar to those of $CaWO_4$. These vibration modes can be classified into external and internal modes, which originate from the lattice phonon (or motion) of [PbO_8] and [MoO_4] clusters, respectively[19]. An isolated [MoO_4] cluster has a T_d cubic symmetry, and its vibrations consist of four internal modes, specified as $\nu_1(A_1)$, $\nu_2(E_1)$, $\nu_3(F_2)$, and $\nu_4(F_2)$, which correspond to the stretching (ν_1 and ν_3) and bending (ν_2 and ν_4) modes, respectively. When these modes exist in the scheelite structure, the size symmetry is reduced to S_4[20,21]. In vibrational infrared modes, only eight stretching and/or bending IR-active vibrational modes are included.

Figure 3 shows the FTIR spectrum of the fishbone-like $PbMoO_4$ nanostructures. The $PbMoO_4$ crystals exhibit an intense absorption band at 780 cm^{-1}, which are ascribed to the ν_3 antisymmetric stretching vibrations of the Mo-O bond in the [MoO_4] clusters. On the other hand, the $\nu_4(F_2)$ modes at around 475 cm^{-1} are attributed to the bending vibrations within the [MoO_4] clusters[22,23]. The weak ν_1 mode at ~920 cm^{-1} is attributed to the symmetric vibration of the [MoO_4] cluster, which is originally IR inactive, thereby confirming the symmetry lowering of [MoO_4] tetrahedrons in the $PbMoO_4$ crystal lattice. Meanwhile, the IR peaks at 975 and 670 cm^{-1} are attributed to the Mo-O and Pb-O stretching modes, respectively. As previously stated, the FTIR spectrum indicates the existence of a well-crystallized $PbMoO_4$. The absence of a bandshift or of peaks that correspond to substructures in the FTIR spectrum indicates that the grown crystals possess FTIR absorption characteristics that are identical to those of $PbMoO_4$.

After the formation of a two-armed structure, the main framework of the fishbone-like crystal is built. The crystal is believed to result from PEG-induced growth effects. The plausible formation mechanism is shown in Fig. 4.

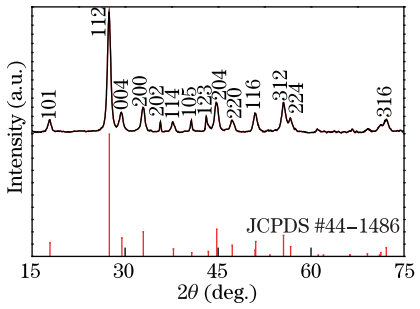

Fig. 2. XRD pattern of the fishbone-like $PbMoO_4$ nanostructures.

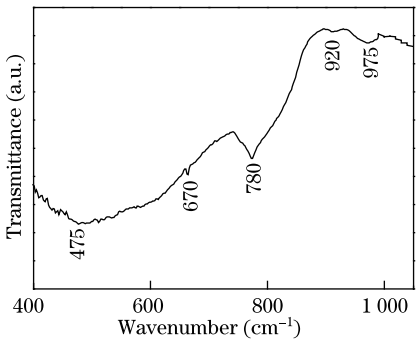

Fig. 3. FTIR spectrum of fishbone-like $PbMoO_4$ nanostructures.

The $PbMoO_4$ nanocrystals in the PEG medium exhibit an "oriented attachment" and is significantly different from the previously reported plate-like products, which were driven only by their own crystal nature[24,25]. Oriented aggregation is considered an important crystal growth mechanism in both aqueous and nonaqueous solutions[26]. Bonding between the particles reduces the overall energy by removing the surface energy associated with unsatisfied bonds.

The growth of the $PbMoO_4$ fishbone through the oriented attachment of nanoparticles is preferentially along specified crystallographic directions. The exact reason for this unique structure is unclear. However, the PEG2000 surfactant may be a key element in this process, as indicated by the absence of dendrites when the reaction is performed without PEG2000[24]. Thus, the adherence of PEG2000 molecules to the crystal planes of the $PbMoO_4$ nanoparticles may be occurring at an early crystal growth stage, which can result in the inhibition of further nanoparticle growth.

Given the exponential relationship of the crystal growth rates and the corresponding crystal face energies, the crystals preferentially grow along the direction of the crystal face with the maximum energy and exhibit the rod-like stem structures. In this case, the PEG molecules are absorbed on the crystal face with the higher negative-charge density (high-index). Thus, the desorption of PEG2000 molecules from specific planes become more difficult as a result of violent thermal disturbance, which results in the exposure of low-index surfaces and leads to an increase in the total energy of the system. To conform to the principle of minimum energy, $PbMoO_4$ secondary nanorods gradually grow on two sides of the stem along the stem direction and eventually form the fishbone structures.

Figure 5 shows the room-temperature PL emission spectrum of the fishbone-like $PbMoO_4$ nanostructures. When excited at 250 nm, the as-prepared $PbMoO_4$ nanopowders exhibit PL emissions in a broad wavelength range. The maxima are at 4.05 eV (306 nm) and 3.18 eV (390 nm), which are blueshifted compared with literature results[27]. Given that the nature of the optical transitions of $PbMoO_4$ remain unclear, these two PL emission bands may have originated from Pb^{3+} and O^- hole centers based on previous reflectivity measurements as well as on current knowledge of their electronic structures. The top level of the valence band of the lowest unoccupied states consists of 4d Mo states that are split into two sets of bands with e (primarily Mo 4d) and t (primarily O 2p) symmetries. Thus, the PL emission bands correspond to the electron transitions from the valence O 2p states to the Mo 4d states, which have different symmetries[28].

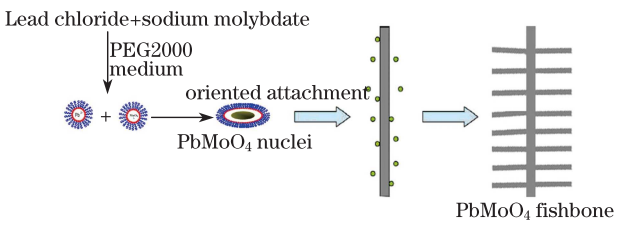

Fig. 4. Schematic growth diagram of the fishbone-like $PbMoO_4$ nanostructures.

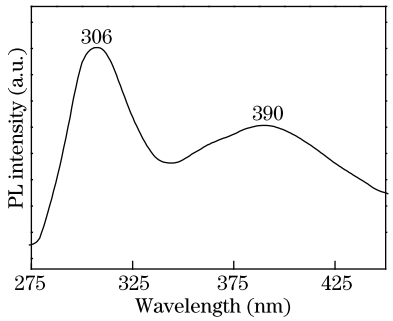

Fig. 5. PL spectrum of the fishbone-like $PbMoO_4$ nanostructures.

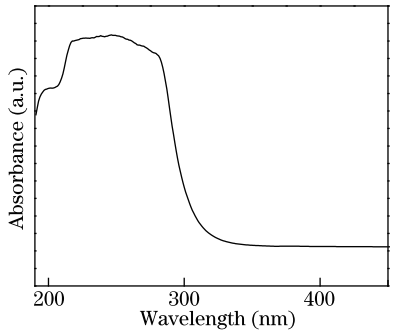

Fig. 6. UV-Vis absorption spectrum of the fishbone-like $PbMoO_4$ nanostructures.

The UV-Vis absorption spectrum of the fishbone-like $PbMoO_4$ nanostructures is shown in Fig. 6. The absorption of $PbMoO_4$ exhibits a noticeable blueshift compared with that of the bulk sample. This blueshift can be attributed to nanosize effects[29]. Moreover, the absorption edge is in the 280 to 310 nm region. This absorption is attributed to a charge-transfer transition, in which an oxygen 2p electron transfers to one of the empty Mo 5d orbital. The excitation from O_{2p} to Mo_{5d} in the $[MoO_4]$ group results in the absorption of ultraviolet radiation by $PbMoO_4$. In the excited state of the $[MoO_4]$ group, the hole (on the O) and the electron (on the Mo) remain paired during excitation because of their strong interaction.

The band gap of a material is related to the absorbance and photon energy. The direct-transition band gap of crystalline tetragonal $PbMoO_4$ can be calculated by extrapolating the linear portion of the plot of $(\alpha h\nu)^2$ against the photon energy ($h\nu$) to 0. The obtained result is shown in Fig. 7 and listed in Table 1. The table also shows the E_{gap} values for $PbMoO_4$ formed via other methods[30,31].

The estimated E_{gap} value obtained in this study (4.07 eV) is a slightly higher than previously reported data. E_{gap} is associated with the presence of intermediary energy levels within the band gap, which depend on the degree of structural order-disorder in the lattice[28]. Thus, the increase in structural organization leads to a reduction in these intermediary energy levels, which results in an increase in the E_{gap} value. The previously reported E_{gap} value (4.7 eV)[26] is the largest and is attributed to the presence of Mn^{3+} ions in $PbMoO_4$. This E_{gap} leads to an increase in the energy levels within the

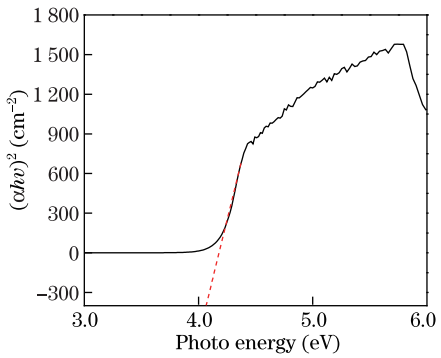

Fig. 7. Plot of $(\alpha h\nu)^2$ against the photon energy ($h\nu$) of the fishbone-like $PbMoO_4$ nanostructures.

Table 1. Comparative E_{gap} Values of the $PbMoO_4$ Obtained in This Work and Those Previously Synthesized in Literature via Different Synthesis Methods

Method	Temperature (°C)	Time (min)	E_{gap} (eV)
Chemical	900	1 800	2.94
Conventional Hydrothermal	120	10	3.19
Czocharalski	1 000	1 440	3.58
Linear-Augmented-Plane-Wave	–	–	3.62
Hydrothermal-Sonochemical	160	160	3.95
Numerically Discrete Variational	–	–	4.7
This Work	160	240	4.07

forbidden band region.

In conclusion, a PEG2000 surfactant-assisted hydrothermal method is used to prepare fishbone-like $PbMoO_4$ nanostructures, in which numerous secondary branches vertically grow on both sides of the main stem. The results show that the molecular nature of PEG2000 significantly affects the $PbMoO_4$ nanoparticle morphologies and sizes, particularly when compared with the products obtained in aqueous media. The XRD and FTIR results both indicate that the particles exhibit a scheelite-type tetragonal structure. The UV-Vis absorption edge of the $PbMoO_4$ nanofishbones is in the 280 to 310 nm region, and the band gap is 4.07 eV. When excited at 250 nm, the particles exhibit broad PL emission bands with the maxima at 306 and 390 nm. $PbMoO_4$ nanocrystals in PEG medium orientedly grow and form rod-like stem, which leads to an increase of total energy of the system. To meet the princle of minimum energy, $PbMoO_4$ secondary nanorods grow gradually on two sides of the stem, and thus yield final fishbones.

This work was supported by the National Natural Science Foundation of China (No. 21106083), the Shanghai Municipality Education Committee Foundation (Nos. 10YZ182 and 09ZZ196), and the Shanghai Leading Academic Discipline Project (No. J51504).

References

1. D. Singh, B. Sirota, S. Talpatra, P. Kohli, C. Rebholz, and S. Aouadi, J. Nanopart. Res. **14,** 781 (2012).
2. Y. Guo, G. Fan, Z. Huang, J. Sun, L. Wang, T. Wang, and J. Chen, Thermochim. Acta **530,** 116 (2012).
3. V. Marques, L. Cavalcante, J. Sczancoski, A. Alcântara, M. Orlandi, E. Moraes, E. Longo, J. Varela, M. Siu Li, and M. Santos, Cryst. Growth Des. **10,** 4752 (2010).
4. G. J. Xing, R. Liu, C. Zhao, Y. L. Li, Y. Wang, and G. M. Wu, Ceram. Intern. **37,** 2951 (2011).
5. D. Errandonea, D. Santamaria-Perez, V. Grover, S. Achary, and A. Tyagi, J. Appl. Phys. **108,** 073518 (2010).
6. D. Hernández-Uresti, A. Martínez-de la Cruz, and L. M. Torres-Martínez, Res. Chem. Intermediat **38,** 817 (2012).
7. Q. C. Chen and Q. S. Wu, Catal. Commun. **24,** 85 (2012).
8. A. Y. Neiman, A. F. Guseva, and A. R. Sharafutdinov, Solid State Ionics **101,** 367 (1997).
9. H. Zeng, J. Cryst. Growth **171,** 136 (1997).
10. V. M. Longo, L. S. Cavalcante, E. C. Paris, J. C. Sczancoski, P. S. Pizani, M. S. Li, J. Andrés, and E. Longo, J. Phys. Chem. C **115,** 5207 (2011).
11. J. Bi, L. Wu, Y. Zhang, Z. Li, J. Li, and X. Fu, Appl. Catal. B **91,** 135 (2009).
12. A. Phuruangrat, T. Thongtem, and S. Thongtem, J. Cryst. Growth **311,** 4076 (2009).
13. L. S. Cavalcante, J. C. Sczancoski, R. L. Tranquilin, J. A. Varela, E. Longo, and M. O. Orlandi, Particuology **7,** 353 (2009).
14. M. Hashim, C. Hu, X. Wang, X. Li, and D. Guo, Appl. Surf. Sci. **258,** 5858 (2012).
15. F. Danevich, B. Grinyov, S. Henry, M. Kosmyna, H. Kraus, N. Krutyak, V. Kudovbenko, V. Mikhailik, L. Nagornaya, and B. Nazarenko, Nuclear Instruments and Methods in Physics Research Section A **622,** 608 (2010).
16. J. Sczancoski, M. Bomio, L. Cavalcante, M. Joya, P. Pizani, J. Varela, E. Longo, M. S. Li, and J. Andrés, J. Phys. Chem. C **113,** 5812 (2009).
17. Powder diffraction File JCPDS Int. Centre Diffraction Data, PA 19073-3273, USA (2001).
18. J. Yang, C. Zhang, L. Wang, Z. Hou, S. Huang, H. Lian, and J. Lin, J. Solid State Chem. **181,** 2672 (2008).
19. L. S. Cavalcante, V. M. Longo, J. C. Sczancoski, M. A. P. Almeida, A. A. Batista, J. A. Varela, M. O. Orlandi, E. Longo, and M. S. Li, Cryst. Eng. Commun. **14,** 853 (2012).
20. T. Thongtem, A. Phuruangrat, and S. Thongtem, J. Ceram. Process. Res. **9,** 189 (2008).
21. T. Thongtem, A. Phuruangrat, and S. Thongtem, Curr. Appl. Phys. **8,** 189 (2008).
22. J. Sczancoski, L. Cavalcante, N. Marana, R. Da Silva, R. Tranquilin, M. Joya, P. Pizani, J. Varela, J. Sambrano, and M. Siu Li, Curr. Appl. Phys. **10,** 614 (2010).
23. A. Phuruangrat, N. Ekthammathat, T. Thongtem, and S. Thongtem, J. Phys. Chem. Solids **72,** 176 (2011).
24. R. Jia and Y. Zhang, Chin. Opt. Lett. **8,** 1152 (2010).
25. J. Silver, M. Martinez-Rubio, T. Ireland, G. Fern, and R. Withnall, J. Phys. Chem. B **105,** 948 (2001).
26. Y. Cheng, Y. S. Wang, D. Q. Chen, and F. Gao, J. Phys. Chem. B **109,** 794 (2005).
27. F. Q. Dong and Q. S. Wu, Appl. Phys. A **91,** 161 (2008).
28. D. A. Spasskya, S. N. Ivanov, V. N. Kolobanov, V. V. Mikhailin, V. N. Zemskov, B. I. Zadneprovski, and L. I. Potkin, Radiat. Meas. **38,** 607 (2004).
29. G. Z. Shen, Y. Bando, and D. Golberg, J. Phys. Chem. B **110,** 20777 (2006).
30. M. A. P. Almeida, L. S. Cavalcante, M. Siu Li, J. A. Varela, and E. Longo, J. Inorg. Organomet. Polym. Mater. **22,** 264 (2012).
31. J. Y. Chen, Q. R. Zhang, T. Y. Liu, and Z. X. Shao, Phys. B **403,** 555 (2008).